

Spatial extent of oxygen metabolism and hemodynamic changes during functional activation of the rat somatosensory cortex

Andrew K. Dunn,* Anna Devor, Anders M. Dale, and David A. Boas

Martinos Center for Biomedical Imaging, Massachusetts General Hospital, Harvard Medical School, 149 13th Street, Charlestown, MA 02129, USA

Received 3 September 2004; revised 16 February 2005; accepted 5 April 2005

Available online 31 May 2005

The spatial extent of the changes in oxy-hemoglobin (HbO), deoxy-hemoglobin (HbR), total hemoglobin concentration (HbT), cerebral blood flow (CBF), and the cerebral metabolic rate of oxygen (CMRO₂) in response to forepaw and whisker stimulation were compared in the rat somatosensory cortex using a combination of multi-wavelength reflectance imaging and laser speckle contrast imaging of cerebral blood flow. The spatial extents of the response of each hemodynamic parameter and CMRO₂ were found to be comparable at the time of peak response, and at early times following stimulation onset, the spatial extent of the change in HbR was smaller than that of HbO, HbT, CBF, and CMRO₂. In addition, a slight spatial dependence was found in the power law coefficient relating changes in CBF and HbT. Although the CMRO₂ response is a metabolic measure and thus expected to have a more localized response than the hemodynamic parameters, the results presented here suggest that this may not be the case in general, possibly due to the increased sensitivity of optical imaging techniques to superficial cortical layers where the lateral extent of the metabolic and neuronal activation is larger compared to that in layer IV. In addition, we found that the measured spatial extent of the CMRO₂ changes was insensitive to assumptions made in the calculation of the CMRO₂ changes such as baseline hemoglobin concentrations, vascular weighting constants, and wavelength dependence of tissue scattering. Multi-parameter full field imaging of the functional response provides a more complete picture of the hemodynamic response to functional activation including the spatial and temporal estimation of CMRO₂ changes.

© 2005 Elsevier Inc. All rights reserved.

Keywords: Hemodynamic changes; Hemoglobin; Oxygen metabolism

Introduction

The relationship between the hemodynamic and metabolic responses has been the subject of great interest since the PET measurements by Fox and Raichle (Fox and Raichle, 1986; Fox

et al., 1988) who found that focal increases in cerebral blood flow (CBF) were roughly 6 times greater than that in the cerebral rate of metabolic oxygen (CMRO₂). Much of this interest has been driven recently by the fact that the BOLD fMRI signal is dependent on the changes in CBF, cerebral blood volume (CBV), and CMRO₂. Therefore, in order to fully understand the origins of the BOLD signal, the individual dynamics and relationships between the changes in each of the hemodynamic and metabolic parameters must be better understood.

Despite the recent interest in imaging CMRO₂ changes during brain activation, the spatial extent of the CMRO₂ changes has not been investigated in detail. Deoxyglucose autoradiographic analysis of glucose metabolism changes in response to functional activation in rats (McCasland and Woolsey, 1988) and monkeys (Tootell et al., 1988) has revealed that the metabolic changes are well localized to the functional architecture of the cortex in layer IV. However, mapping techniques based on hemodynamic changes, such as optical imaging of intrinsic signals and fMRI, typically reveal less localized responses due to vascular overspill phenomenon (Brett-Green et al., 2001; Erinjeri and Woolsey, 2002; Grinvald et al., 1994; Tootell et al., 1997). In this paper, we sought to investigate whether the CMRO₂ changes in the rat somatosensory cortex were more localized than the accompanying hemodynamic changes using combined laser speckle contrast imaging of CBF and multi-wavelength reflectance imaging of HbO, HbR, and HbT.

Due to limitations of the various functional brain imaging techniques such as fMRI, PET, and optical imaging, simultaneous measurement of all of the parameters necessary for calculation of CMRO₂ changes has been challenging. To overcome these limitations, various assumptions and models about the relationships between hemodynamic and metabolic parameters have been proposed (Buxton et al., 1998; Hyder et al., 1998; Jones et al., 2001; Mandeville et al., 1999). In particular, for fMRI and optical imaging, the relationship between CBF and CBV is often assumed since these parameters are not typically measured simultaneously.

Recently, both optical (Culver et al., 2003; Durduran et al., 2004b; Jones et al., 2001, 2002; Mayhew et al., 2001) and fMRI techniques (Hoge et al., 1999; Kida et al., 2000; Lu et al., 2003)

* Corresponding author. Fax: +1 617 726 7422.

E-mail address: adunn@nmr.mgh.harvard.edu (A.K. Dunn).

Available online on ScienceDirect (www.sciencedirect.com).

have been developed that enable simultaneous measurements of multiple hemodynamic measures in order to reduce the reliance on model assumptions in the determination of CMRO₂ changes. Despite these methodological advances, the spatial extent of the stimulus-induced CMRO₂ changes has not been investigated in detail due to limitations in the spatial resolution of these techniques. For example, by combining laser Doppler flowmetry measurements of CBF with reflectance spectroscopy to determine the changes in oxyhemoglobin (HbO), deoxyhemoglobin (HbR), and total hemoglobin concentrations (HbT), the temporal dynamics of CMRO₂ changes were investigated at a single spatial location during functional activation in rats (Jones et al., 2001, 2002; Mayhew et al., 2001; Sheth et al., 2004a). Another approach to measure CMRO₂ changes was to simultaneously measure CBF using laser Doppler flowmetry and microvascular oxygen tension using oxygen-dependent phosphorescence quenching during forepaw stimulation in rats (Ances et al., 2001). Although these studies provided detailed information about the temporal dynamics of the CMRO₂ changes, it was not possible to examine the spatial dynamics of the CMRO₂ changes since these were point measurements at a single spatial location.

To obtain information about the spatial response to functional stimulation, optical imaging of intrinsic signals is commonly used. This method has provided numerous insights into the functional organization of the cortex (Grinvald et al., 1986; Masino and Frostig, 1996; Masino et al., 1993; Ts'o et al., 1990) by mapping the changes in cortical reflectance arising from the hemodynamic changes that accompany functional stimulation. The majority of these studies have been based on qualitative mapping at a single wavelength, and while they have provided valuable insight into many aspects of cortical function, the techniques used in these studies have been unable to reveal quantitative spatial information about the individual hemodynamic (HbO, HbR, HbT) and metabolic (CMRO₂) components that underlie the measured signals. This is due to the fact that images at multiple wavelengths must be combined to quantify hemoglobin concentrations, and most intrinsic optical imaging is done at only a single wavelength band. Acquisition of this spectroscopic information has been achieved only by sacrificing spatial information (Malonek and Grinvald, 1996; Mayhew et al., 2000), which has precluded full field imaging of HbO, HbR, and HbT. While a few studies have utilized intrinsic optical imaging at more than one wavelength (Ba et al., 2002; Sheth et al., 2003, 2004b), the spectral information was acquired in separate trials and was not combined with a physical model of light propagation through tissue to quantify the spatiotemporal changes in hemoglobin concentrations and oxygenation.

Recently, we have developed a spectroscopic imaging method that enables full field imaging of reflectance changes at multiple wavelengths by rapid switching of the illumination wavelength using a continuously rotating filter wheel (Dunn et al., 2003). This technique allows quantitative imaging of the concentration changes in HbO, HbR, and HbT with the same spatial and temporal resolution as traditional intrinsic optical imaging. We have used this instrument to study the relationship between the hemodynamic changes and electrical activity during whisker stimulation in rats by combining the imaging technique with simultaneous electrophysiology recordings (Devor et al., 2003, 2005).

Traditionally, the CBF response to functional activation has been studied using laser Doppler flowmetry, which only provides information about the CBF changes at a single spatial location. Scanning laser Doppler has also been used to provide images of activation-induced changes in CBF (Ances et al., 1999) but is limited in both its spatial and temporal resolutions. More recently, laser speckle contrast imaging of CBF (Dunn et al., 2001) has been used for imaging the CBF response under a number of physiological conditions in animal models (Ayata et al., 2004; Bolay et al., 2002; Dunn et al., 2003; Durduran et al., 2004a; Kharlamov et al., 2004). Laser speckle contrast imaging enables high spatiotemporal resolution imaging of blood flow changes using relatively simple instrumentation by analyzing the alterations in the laser speckle pattern caused by the motion of the blood cells (Briers et al., 1999).

In this paper, we examined whether the spatial extent of CMRO₂ changes during forepaw and whisker stimulation is more localized than the changes in CBF, HbO, HbR, and HbT using a combination of multi-wavelength reflectance imaging and laser speckle contrast imaging of CBF. No significant differences in the spatial extent of the stimulus-induced changes were found between CMRO₂ and the hemodynamic parameters, suggesting that CMRO₂ changes are not necessarily more localized than the hemodynamic measures. In addition, the spatial extent of the CMRO₂ response was insensitive to methodological considerations such as the assumed values for baseline hemoglobin concentrations, vascular weighting constants in the calculation of CMRO₂ changes, and wavelength dependence of tissue scattering.

Materials and methods

Animal preparation

All experimental procedures were approved by the MGH Subcommittee on Research Animal Care. Male Sprague–Dawley rats (250–350 g, $n = 6$) were initially anesthetized with 2% halothane. A tracheotomy was performed to allow artificial ventilation, and cannulas were inserted in the femoral artery and vein. Following surgery, the animals were artificially ventilated with 1.5% halothane, 70% N₂O and 30% O₂. Body temperature was maintained at 37°C with a heating blanket and arterial blood pressure was continuously recorded (100–130 mm Hg) and blood gas and expired CO₂ were monitored ($pO_2 = 130–180$, $pCO_2 = 35–45$). The skull over the somatosensory cortex was thinned with a dental burr until transparent (~100 μm). A well was formed around the thinned portion of the skull using petroleum jelly, and was filled with mineral oil. A glass coverslip was placed over the oil-filled well to create a cranial window for optimal image quality. Subsequently, halothane was discontinued, and anesthesia was maintained with 50 mg/kg bolus of α -chloralose followed by continuous intravenous infusion at 40 mg/kg/h.

Imaging instrument

A schematic illustration of the imaging instrument is illustrated in Fig. 1. The details of the instrument have been described elsewhere (Dunn et al., 2003) and a brief description is provided here. Spectral imaging is achieved by illuminating

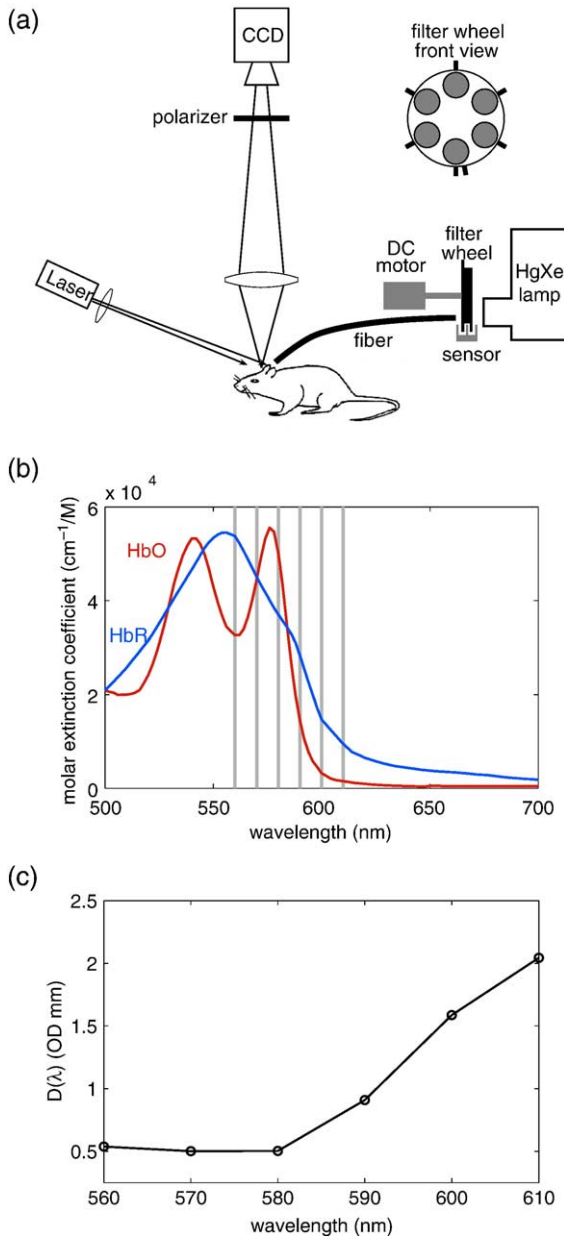


Fig. 1. (a) Schematic of instrument used for multi-wavelength and laser speckle contrast imaging. (b) Extinction spectra of HbO and HbR illustrating the center wavelengths of the six filters used in the multi-spectral imaging. (c) Differential pathlength factor, D_a computed from Monte Carlo simulations.

the cortex with different bands of wavelengths and acquiring images at each illumination band sequentially. Light from a xenon arc lamp passes through 10-nm-wide bandpass filters and is coupled into a 12-mm-diameter fiber optic bundle (Edmund Scientific) for illumination of the cortex. Six different bandpass filters are placed on a six-position filter wheel (Thorlabs), which is mounted on a DC motor. The center wavelength of the filters ranges between 560 and 610 nm at 10-nm intervals as indicated in Fig. 1 which shows the center wavelength of each filter superimposed on the extinction spectra of HbO and HbR.

The motor rotates continuously at 3–5 revolutions/s and an image is acquired by the CCD (Coolsnap fx, Roper Scientific,

1300 × 1030 pixels) as each filter passes by the lamp, resulting in an image acquisition rate of 18–30 Hz as described previously (Dunn et al., 2003). The optical magnification was 0.75–1.0×, and the CCD pixels were binned (3 × 3) such that the final image size was approximately 300 × 300 pixels. For speckle contrast imaging of CBF, a laser diode (785 nm, 70 mW) was used to illuminate the cortex, and raw speckle images were acquired at 20–30 Hz at an exposure time of 5 ms. No pixel binning was used for the speckle images, since binning would lead to a reduction in speckle contrast. The linear polarizer was adjusted to minimize specular reflections from the surface of the oil well. Since the whisker and forepaw representations lie on the lateral convexity of the cortex, it was necessary to orient the optical axis of the camera normal to the surface of this portion of the cortex. This was achieved by tilting the stereotaxic frame at an angle of 10–15° and also tilting the camera to further minimize any deviations from normal.

Stimulation paradigm

All stimulation experiments were done in a block-design fashion with 30 s between stimuli, and both forepaw and whisker stimulation trials were run on each of the 6 animals. Each stimulus block consisted of 1 s of baseline image collection followed by 10 s of stimulation. During forepaw stimulation, electrical pulses of 1 mA were applied for 300 μs at 3 Hz using a stimulus isolation unit. During whisker stimulation, a single whisker was deflected by a computer-controlled piezoelectric transducer at 8 Hz. The whisker was displaced upward and allowed a free return to the resting position.

Spectral image analysis

The image set at each wavelength was averaged across trials and the averaged data were converted to changes in HbO and HbR at each pixel using the modified Beer Lambert relationship,

$$\Delta A(\lambda, t) = (\epsilon_{\text{HbO}}(\lambda)\Delta C_{\text{HbO}}(t) + \epsilon_{\text{HbR}}(\lambda)\Delta C_{\text{HbR}}(t))D(\lambda) \quad (1)$$

where $\Delta A(\lambda, t) = \log(R_o/R(t))$ is the attenuation at each wavelength, R_o and $R(t)$ are the measured reflectance intensities at baseline and some time t , ΔC_{HbO} and ΔC_{HbR} are the changes in concentrations of HbO and HbR, respectively, and ϵ_{HbO} and ϵ_{HbR} are the molar extinction coefficients. Eq. (1) was solved for ΔC_{HbO} and ΔC_{HbR} using a least-squares approach. The differential pathlength factor, $D(\lambda)$, accounts for the fact that each wavelength travels slightly different pathlengths through the tissue due to the wavelength dependence of scattering and absorption in the tissue, and was estimated using the approach of Kohl et al. (2000) through Monte Carlo simulations of light propagation in tissue. To simulate the experimental geometry, photons in a 10-mm-diameter diverging beam (NA = 0.05) were launched into a tissue with uniform scattering properties. Photons exiting the tissue were considered detected if their exit position and direction would result in that photon being imaged onto a single CCD pixel. The wavelength-dependent reflectance, $R(\mu_a(\lambda))$ was calculated from the detected photon pathlengths to determine $D(\lambda)$ (Kohl et al., 2000). Baseline scattering properties were $\mu_s = 100 \text{ cm}^{-1}$ and $g = 0.9$ and were assumed to be constant over the wavelength range considered. Hemoglobin was assumed to be the only chromophores of interest and the baseline absorption coefficient was defined as $\mu_a(\lambda) = \epsilon_{\text{HbO}}(\lambda)C_o^{\text{HbO}} + \epsilon_{\text{HbR}}(\lambda)C_o^{\text{HbR}}$, where C_o^{HbO} and C_o^{HbR} are the

assumed baseline concentrations of oxy- and deoxy-hemoglobin. The computed values of the pathlength factor at each wavelength are plotted in Fig. 1c for baseline concentrations of 60 μM and 40 μM for HbO and HbR, respectively (Jones et al., 2002; Mayhew et al., 2000). These baseline values were assumed for all of the results presented here unless noted otherwise. The influence of these assumed baseline values on the spatial extent of the CMRO₂ changes was also investigated by varying C_o^{HbO} and C_o^{HbR} over the range of 20–200 μM, as described below.

Speckle contrast image analysis

Images of CBF changes were determined by calculating the changes in the speckle contrast in a series of laser speckle images. The speckle contrast is defined as the ratio of the standard deviation to the mean pixel intensities, $\sigma/\langle I \rangle$ within a localized region of the image (Briers, 2001). Each raw speckle image was converted to a speckle contrast image using a sliding window of 7×7 pixels in order to balance the tradeoff between adequate estimates of the speckle contrast and spatial resolution (Briers, 2001). Speckle contrast images were averaged

across trials and the averaged set was converted to relative blood flow ($1 + \Delta\text{CBF}/\text{CBF}_o$) by converting each speckle contrast value to an intensity autocorrelation decay time (Briers, 2001), which was assumed to be inversely proportional to blood flow (Bonner and Nossal, 1981), and dividing by baseline, as described elsewhere (Dunn et al., 2001).

Calculation of CMRO₂ changes

The changes in CMRO₂ were calculated from the images of CBF, total hemoglobin, and deoxy-hemoglobin using the relationship (Jones et al., 2001; Mayhew et al., 2000)

$$1 + r\text{CMRO}_2 = \left(1 + \frac{\Delta\text{CBF}}{\text{CBF}_o}\right) \left(1 + \gamma_r \frac{\Delta\text{HbR}}{\text{HbR}_o}\right) \times \left(1 + \gamma_t \frac{\Delta\text{HbT}}{\text{HbT}_o}\right)^{-1} \tag{2}$$

where the subscript ‘o’ indicates baseline values. The parameters γ_r and γ_t are vascular weighting constants which take into account that the measured changes in hemoglobin are a combination of venous

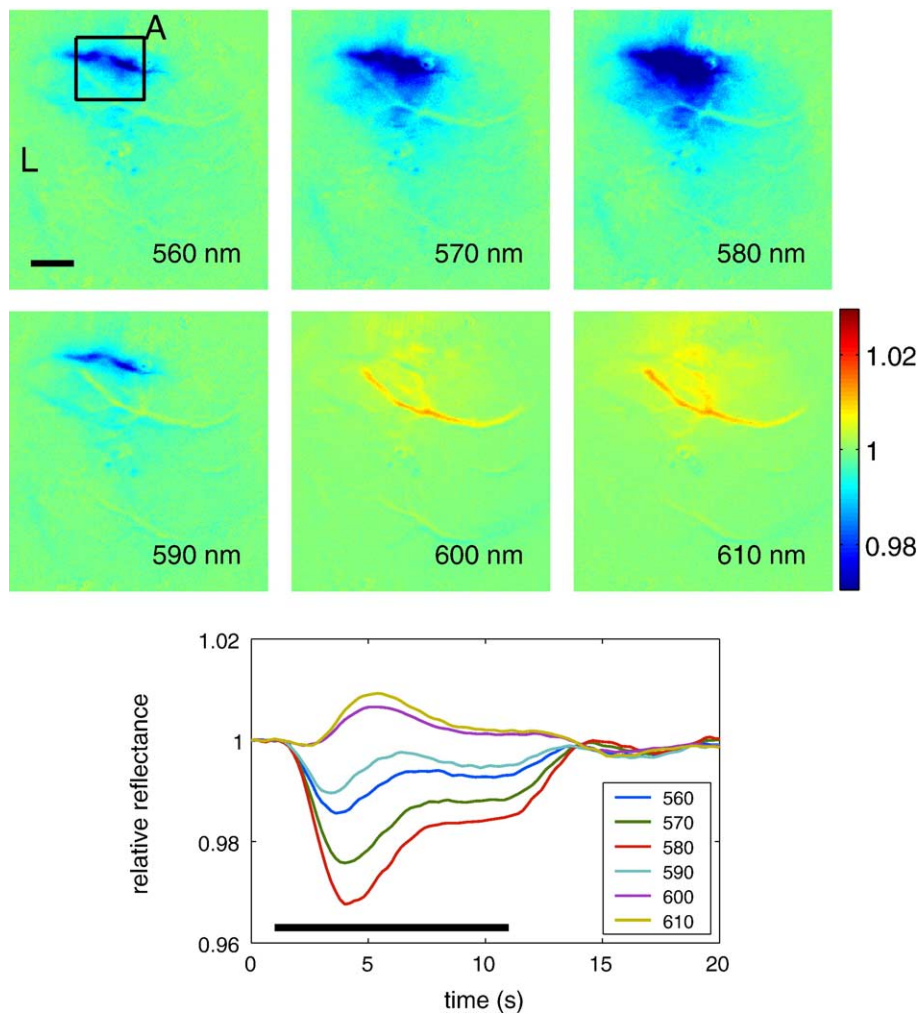


Fig. 2. Example images and timecourses of the relative reflectance changes ($R(t)/R_o$) at the six wavelengths in response to 10 s of forepaw stimulation. The scale bar in the first image corresponds to 1 mm, and the bar in the plot corresponds to the stimulus. The images show the relative reflectance averaged over a 2-s window beginning 2 s after stimulus onset ($3 < t < 5$) (A = anterior, L = lateral).

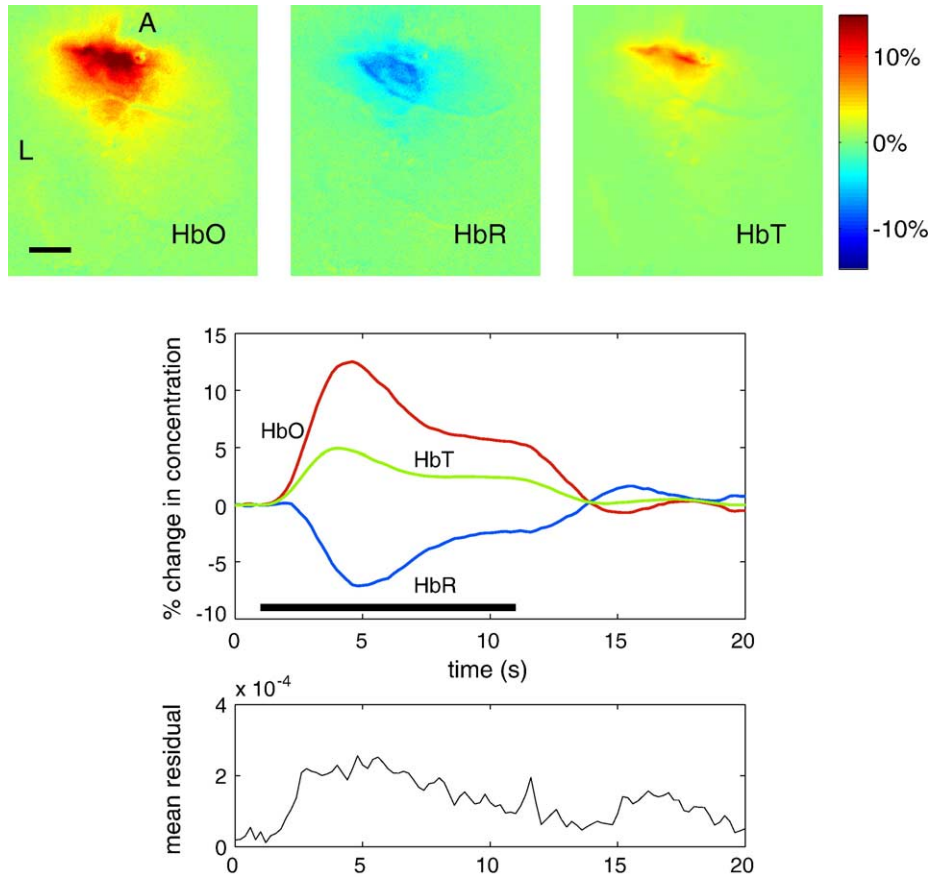


Fig. 3. Timecourses and images of HbO, HbR, and HbT changes (% change from baseline) computed from the multi-wavelength data shown in Fig. 2. The mean residual of the least-squares fit to Eq. (1) is shown in the lower plot. Scale bar in HbO image = 1 mm, A = anterior, L = lateral.

and arterial quantities. This relationship is derived from the standard definition (Hyder, 2004)

$$CMRO_2 = CBF \cdot OEF \quad (3)$$

where OEF is the oxygen extraction fraction. OEF is given by the fractional difference between the arterial and venous oxygen saturation, S_A and S_V , respectively.

$$OEF = \frac{S_A - S_V}{S_A} \quad (4)$$

Under the assumption that $S_A = 1$, this equation simplifies as

$$OEF \approx \frac{HbR_V}{HbT_V} \quad (5)$$

where HbR_V and HbT_V indicate the deoxy- and total hemoglobin concentration in the venules. This model assumes that oxygen extraction is taking place upstream of the venules in the capillaries and arterioles, and that no oxygen extraction is occurring in the venules. Combining Eqs. (3) and (5) and considering changes in each parameter, we arrive at Eq. (2) with the definitions

$$\gamma_r = \frac{\Delta HbR_V}{HbR_{V,o}} \bigg/ \frac{\Delta HbR}{HbR_o} \quad (6)$$

and

$$\gamma_t = \frac{\Delta HbT_V}{HbT_{V,o}} \bigg/ \frac{\Delta HbT}{HbT_o} \quad (7)$$

Our optical measurements average the hemoglobin changes over the arteriole, capillary, and venule compartments and do not provide a direct measure of the changes in the venule compartment. This requires that the γ_r and γ_t be assumed. We test a range of assumed values from 0.5 to 2.

Results

Multispectral imaging of HbO, HbR, and HbT

The spatial changes in reflected light intensity at each of the six wavelengths due to forepaw stimulation are shown in Fig. 2 for one animal averaged over 40 trials. Each image shows the ratio of the

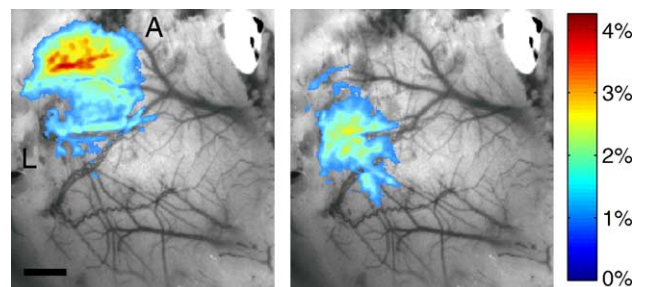


Fig. 4. Comparison of the percent changes in HbT in response to forepaw (left) and whisker (right) stimulation. Scale bar = 1 mm.

reflectance at each wavelength band, averaged over a 2-s interval starting 2 s after stimulation onset, to the average baseline reflectance prior to stimulation. The observed response differs with wavelength, and at wavelengths of 560, 570, 580, and 590 nm, a decrease in reflectance is observed, while at wavelengths of 600 and 610 nm, there is an increase in reflectance. The timecourse of the changes in reflectance at each wavelength, averaged over a 1.75×1.75 mm region of interest centered on the activation (Fig. 2) illustrates the spectral differences in the

temporal response. The largest reflectance change was observed at 580 nm where the total extinction of hemoglobin is largest, while the smallest amplitude changes were observed at 600 and 610 nm.

The corresponding images and timecourses of the changes in HbO, HbR, and HbT are shown in Fig. 3 for the spectral data in Fig. 2, for assumed baseline concentrations of 60 and 40 μM for HbO and HbR, respectively. Also plotted is the mean residual of the least-squares fit of the data to Eq. (1), defined as

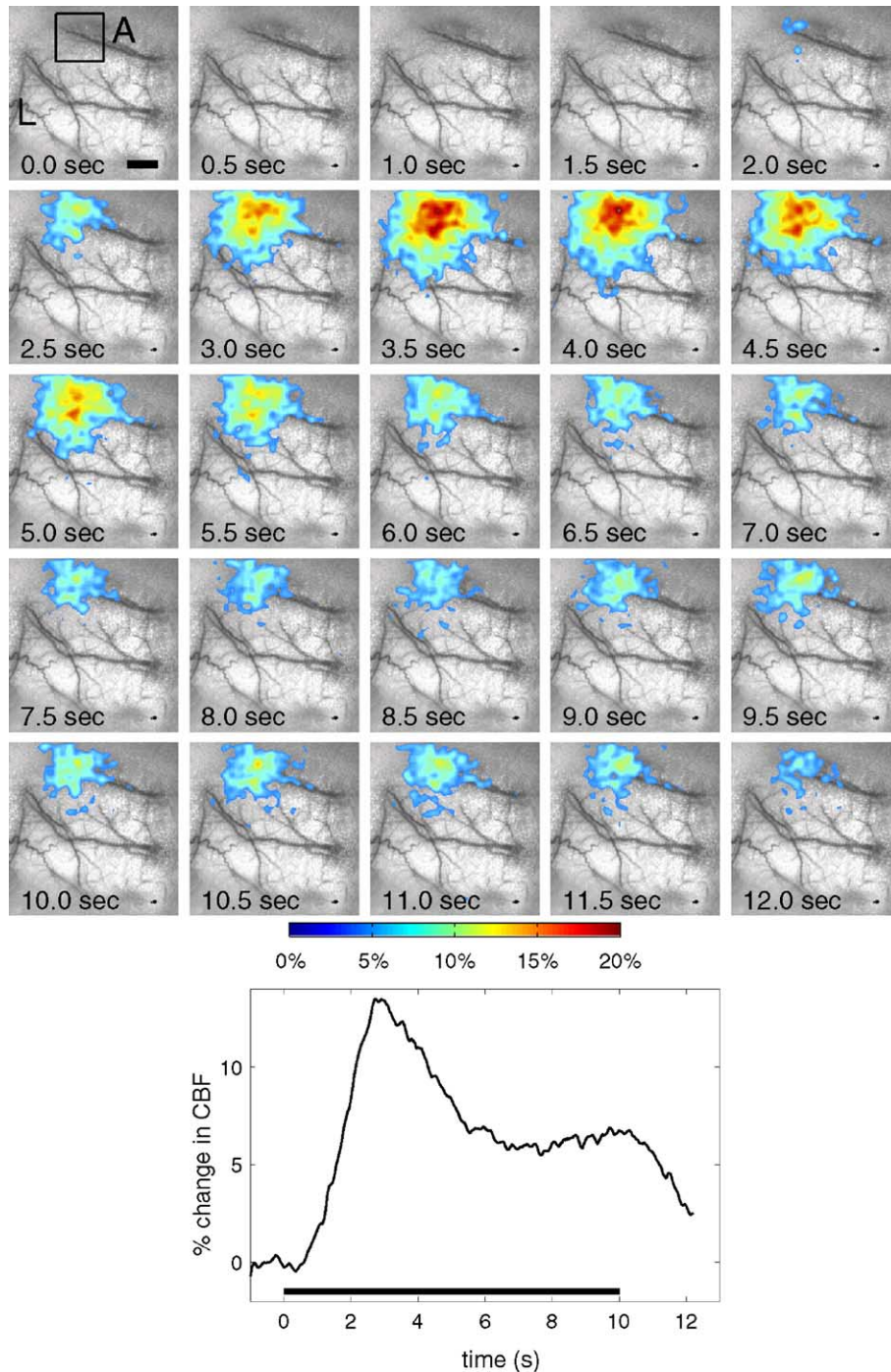


Fig. 5. Percent changes in CBF in response to 10 s of forepaw stimulation. The graph illustrates the percent change in CBF over a 1.75×1.75 mm region of interest centered on the activation (see first image), and the images illustrate the spatial changes at 0.5-s intervals. A = anterior, L = lateral.

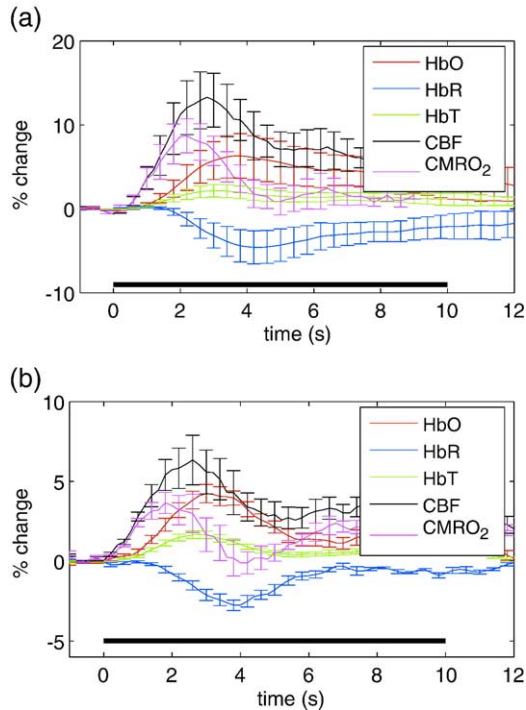


Fig. 6. Timecourse of the average changes in each hemodynamic parameter for forepaw (a) and whisker (b) stimulation.

$1/6 \sum_i |\Delta A_m(\lambda_i, t) - \Delta A_c(\lambda_i, t)|$, where $\Delta A_m(\lambda_i, t)$ and $\Delta A_c(\lambda_i, t)$ are the measured and calculated changes in attenuation. The magnitude of the residual is comparable to that reported by Kohl et al. (2000) who used a large number of wavelengths. Approximately 1 s following the onset of stimulation, an increase in HbO is observed with a delayed decrease in HbR. The spatial responses of HbO, HbR, and HbT illustrate localized increases in HbO and HbT with a co-localized decrease in HbR.

To compare the responses of forepaw and whisker stimulation, each stimulus was repeated in the same animal. The spatial response of HbT averaged 1–3 s following stimulus onset is shown in Fig. 4 for forepaw and whisker stimulation. The changes in HbT greater than 1% are shown superimposed on the vasculature. As expected, the center position of the responses differs between the two stimulus types with the forepaw response located 1.9 mm anterior to the whisker response. The average amplitude of the HbT changes due to forepaw stimulation was found to be 1.8 times greater than for whisker stimulation.

Speckle contrast imaging of CBF

In addition to the changes in hemoglobin concentrations and oxygenation, the changes in CBF during stimulation were also imaged using laser speckle contrast imaging. Fig. 5 illustrates the spatial and temporal changes in CBF following forepaw stimulation averaged over 40 trials in a single animal. The stimulation parameters were the same as those used in Fig. 2. A series of images are shown at 0.5-s intervals, and illustrate a localized increase in CBF beginning approximately 1 s after stimulation onset. The relative changes in CBF are shown superimposed on the vasculature (derived from the speckle contrast image) and the changes in CBF are displayed for all pixels with an increase in CBF greater than 5%. The timecourse of the CBF changes

averaged over a region of interest centered on the activated area illustrates a peak increase in CBF of approximately 12% occurring 3 s after stimulus onset. The initial peak in CBF then decreases to approximately half of its maximum amplitude to a value of ~6%, where it remains until the end of the stimulus, in a manner consistent with previous laser Doppler measurements of CBF during extended forepaw stimulation (Ances et al., 2001).

Combined imaging of CMRO₂ changes

The CMRO₂ changes were calculated from the measured changes in HbR, HbT, and CBF using Eq. (1) with γ_r and γ_t set to 1. For each animal, speckle and multi-spectral image sets were acquired on consecutive trials. The average timecourse of the changes in HbO, HbR, HbT, CBF, and CMRO₂ for both forepaw and whisker stimuli are plotted in Fig. 6, where the timecourses have been averaged over 6 animals. The CMRO₂ timecourse reveals an initial peak increase in CMRO₂ followed by a prolonged plateau in a manner similar to the CBF response. The average amplitude of the plateau in the CMRO₂ response is only slightly above baseline (1.8% and 1.2% for forepaw and whisker, respectively). We note that Eq. (1) is valid under steady state conditions, and we also tested a dynamic CMRO₂ model (Hoge et al., 2005) which did not alter our results.

The times for each parameter to reach its peak value following stimulus onset are listed in Table 1. CMRO₂ reaches its peak response at the earliest time (2.2 and 1.9 s for forepaw and whisker stimuli, respectively) and CBF and HbT both peak approximately 0.5 s after CMRO₂. The HbR response reaches its maximum amplitude at the latest time. All of the parameters were found to reach their maximum values slightly earlier for whisker stimulus than forepaw stimulus.

Fig. 7 illustrates the spatial changes in each hemodynamic parameter averaged over 40 trials of forepaw stimulus in a single animal. The responses of each parameter, shown superimposed on the vasculature, have been thresholded at 1/3 of the maximum response for that parameter, and averaged over a 1-s window around the time of the peak response. All of the hemodynamic parameters show a localized area of activation centered on the same location. The HbR response extends away from the center of activation along a draining vein. In addition, no change in HbR concentration is observed over an area corresponding to a small arterial branch running through the activation area.

Spatial extent of activation

The spatial extent of the response of each hemodynamic parameter was estimated by fitting a two-dimensional Gaussian

Table 1
Times to peak response following stimulus onset for each hemodynamic and metabolic parameter

Parameter	Forepaw stimulation (s)	Whisker stimulation (s)
rCMRO ₂	2.2	1.9
CBF	2.8	2.7
HbT	3.0	2.8
HbO	3.5	3.0
HbR	4.3	3.8

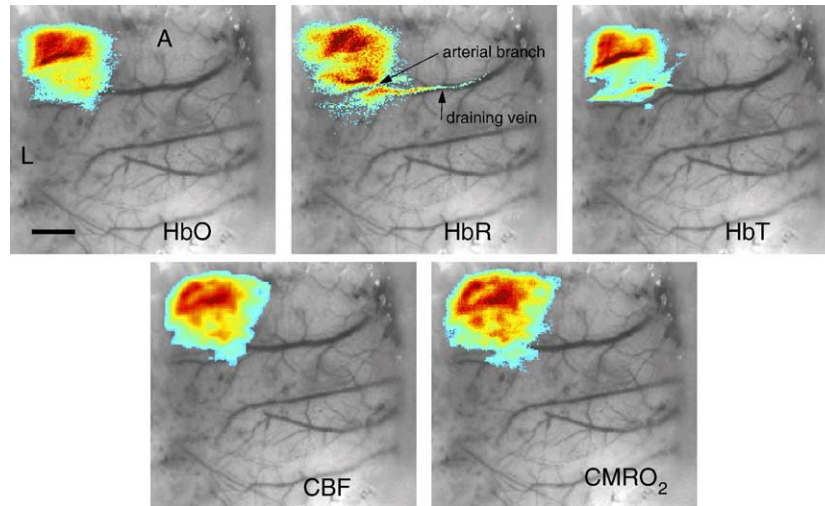


Fig. 7. Spatial changes in HbO, HbR, and HbT concentrations, as well as the changes in CBF and CMRO₂ in a single animal following forepaw stimulation using combined multi-spectral and laser speckle contrast imaging. The responses of each parameter is shown superimposed on the vasculature and have been thresholded at 1/3 of the maximum response for that parameter, and averaged over a 1-s window centered around the time of the peak response (A = anterior, L = lateral, scale bar = 1 mm).

profile to the average spatial response for each parameter, which was obtained by averaging the response over a 1-s window centered on the time of the maximum response. The width of the Gaussian profile was then used to compute the area of the response. The average spatial extent of each parameter at the time of peak response for that parameter is shown in Figs. 8a and b for both forepaw and whisker stimulation, respectively.

The spatial extents of each parameter at the time of the peak response are approximately equal for forepaw stimulation, but show more variability for whisker stimulation. In particular, the measured spatial extents of the CBF and CMRO₂ changes are slightly larger than the other parameters for whisker stimulation. While the spatial extents of each parameter at the time of peak response are approximately the same for forepaw stimulation, differences in the spatial extents were found at early times. Fig. 8c shows the average spatial extent of each parameter 1–2 s after stimulation onset for forepaw stimulation. All parameters demonstrated a smaller spatial extent than at the time of peak response, suggesting a more localized response at early times. The average spatial extents of the changes in CMRO₂, CBF, HbO, and HbT were larger than HbR at this early time.

Discussion

Spatial extent of hemodynamic and metabolic responses

The spatial extent of the hemodynamic and metabolic responses is an important consideration for functional mapping of the cortex and in addressing the question of neurovascular coupling in the brain. Since the CMRO₂ response is a measure of oxygen metabolism, we initially hypothesized that CMRO₂ would demonstrate a more localized response than the hemodynamic parameters since the spatial extent of glucose metabolism changes in layer IV of the cortex (Durham and Woolsey, 1985; Kossut et al., 1988; McCasland and Woolsey, 1988; Tootell et al., 1988) is typically well localized, whereas the spatial extent of functional activation obtained with hemodynamic techniques

such as BOLD fMRI (Saad et al., 2003) and optical imaging (Brett-Green et al., 2001; Grinvald et al., 1994; Erinjeri and Woolsey, 2002) is often distributed over a larger area because of vascular overspill. In contrast to the glucose metabolism changes, however, the spatial extent of the neuronal activity, imaged with voltage-sensitive dyes, is comparable to the spatial extent of the hemodynamic response imaged with intrinsic optical imaging (Kleinfeld and Delaney, 1996; Slovins et al., 2002). In this study, we found that the CMRO₂ response has approximately the same spatial extent as the hemodynamic parameters at the time of peak response (Fig. 8a), and at early times relative to stimulation onset, the spatial extent of the CMRO₂ change was slightly larger than that of the other parameters (Fig. 8c). The large spatial extent of the CMRO₂ changes compared with the reported spatial extents of glucose utilization could be due to the fact that the sensitivity of the optical imaging techniques used here is more heavily weighted to the superficial layers of the cortex where the lateral extent of the metabolic and neuronal changes is more spread out than in layer 4 (Kossut et al., 1988).

The CMRO₂ response is calculated from the measured changes in CBF, HbR, and HbT by assuming values for the vascular weighting constants, γ_r and γ_t , as well as the baseline concentrations of HbO and HbR. Each of these assumed parameters potentially could affect the spatial characteristics of the calculated CMRO₂ response. Therefore, the effect of each of these assumed quantities on the calculated spatial extent of CMRO₂ change was examined by varying each quantity and computing the change in the spatial extent of the CMRO₂ response. Fig. 9 shows the effect of γ_r and γ_t on the spatial extent of the CMRO₂ change where the values have been normalized to the spatial extent when $\gamma_r = 1$ and $\gamma_t = 1$. The spatial extent varies by only a few percent over the range of $\gamma = 0.5$ – 2 , which spans the expected physiologic range for γ_r and γ_t (Jones et al., 2001), suggesting that the vascular weighting constants do not substantially influence the spatial extent of the calculated CMRO₂ response.

The assumed values of the baseline concentrations of HbO and HbR (and therefore HbT), which affect the amplitude of the

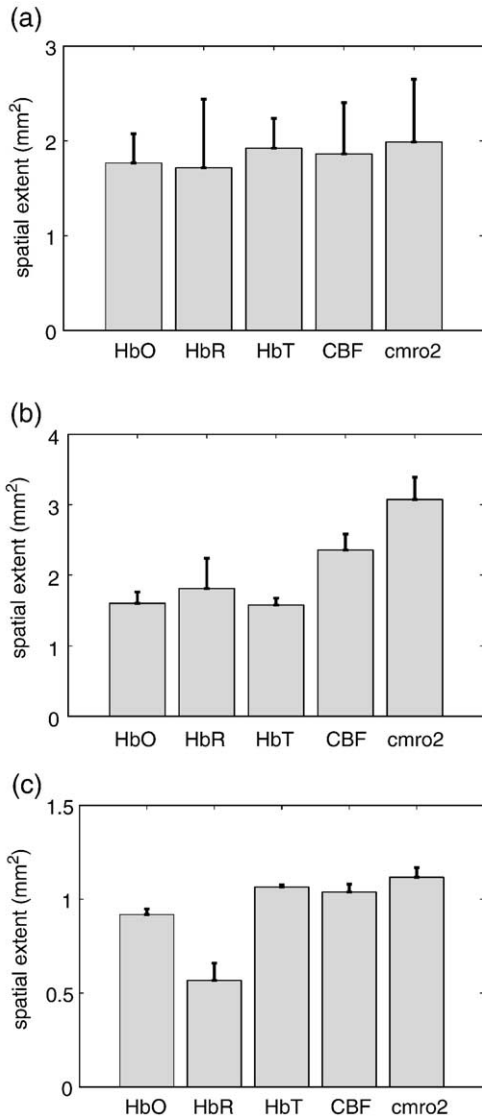


Fig. 8. Calculated spatial extent of each hemodynamic parameter at the time of peak response for forepaw (a) and whisker (b) stimulation. The graph in panel (c) shows the spatial extent of the response 1–2 s following stimulus onset for forepaw stimulus.

changes in HbO, HbR, and HbT as well as the differential pathlength factor, also were found to have a small effect on the spatial extent of the CMRO₂ changes (Fig. 10). The spatial extent of the CMRO₂ response has been normalized to its value at baseline concentrations of 40 and 60 μM for HbR and HbO, respectively. The calculated spatial extent of the CMRO₂ changes was found to vary by only a few percent as the baseline concentrations of HbR and HbO were varied over the range of 20–200 μM. Therefore, the spatial response of CMRO₂ appears to be insensitive to the assumed baseline HbR concentration and oxygen saturation, which are typically unknown parameters.

Another consideration in the determination of CMRO₂ changes from measurements of HbR, HbT, and CBF using a combination of multi-wavelength reflectance imaging and laser speckle contrast imaging is that the wavelength of light differs slightly across these measurements. Since the scattering properties of tissue are wavelength dependent, the depth of sampling of the tissue will also vary

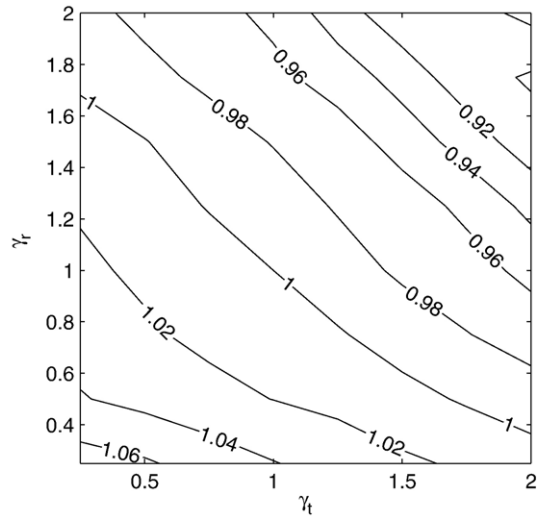


Fig. 9. Effect of the vascular weighting constants, γ_r and γ_t , on the spatial extent of the CMRO₂ response for forepaw stimulation. Contour levels show the ratio of the spatial extent at a particular γ_r , γ_t to the spatial extent at $\gamma_r = 1$, $\gamma_t = 1$.

slightly, which could lead to partial volume errors (Fabricius et al., 1997; Kohl et al., 2000; Strangman et al., 2003). To estimate the effects of the wavelength-dependent optical properties on the sampling depth of the detected light, our Monte Carlo model was used to compute the sampling depth at scattering coefficients of 100 and 150 cm⁻¹, corresponding to the longest and shortest wavelengths in our measurements (785 and 560 nm). The average sampling depths were 0.45 mm at $\mu_s = 150$ cm⁻¹ and 0.6 mm at $\mu_s = 100$ cm⁻¹ ($g = 0.9$), while the lateral extent of the photon sampling was approximately the same at both wavelengths (0.15 mm FWHM). Previously, Gerrits et al. (2000) reported that the changes in CBF during whisker stimulation occur primarily at the surface of the cortex (<0.5 mm), suggesting that all of the wavelengths used in the current study were sensitive to the majority of the hemodynamic changes. Although the values of the scattering coefficient of cortical tissue at these wavelengths are not known precisely, the difference in μ_s is unlikely to be greater than 50% based on previous estimates of the optical properties of

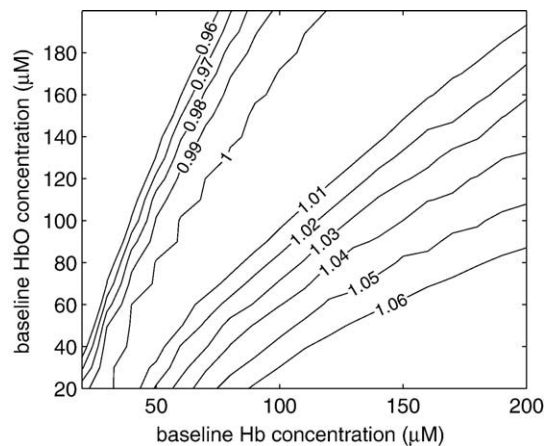


Fig. 10. Effect of baseline concentration of HbO and HbR on the spatial extent of the CMRO₂ response for forepaw stimulation. The values have been normalized to $C_o^{HbO} = 60$ μM and $C_o^{Hb} = 40$ μM.

cortical tissue (Bevilacqua et al., 1999; Matcher et al., 1997). These previous estimates were limited to near-infrared wavelengths, but extrapolation of both of these reports to the wavelength range of 560–785 nm by assuming a wavelength dependence of $A\lambda^{-b}$ ($A = 91$, $b = 0.34$) (Graaff et al., 1992) suggests that the difference in scattering coefficient is less than 20% over this range, which would result in a smaller difference in the sampling depth of the CBF and multi-wavelength measurements. Therefore, our estimate of the differences in sampling depths (0.45 vs. 0.6 mm) represents a worst-case scenario. In addition, the variation in sampling depth in our measurements due to the wavelength dependence of tissue scattering is likely to be less severe than the sampling depth variations that arise in simultaneous laser Doppler flowmetry and optical spectroscopy measurements of CMRO₂ (Jones et al., 2001; Mayhew et al., 2001) due to the different illumination and detection geometries of LDF and optical spectroscopy.

Temporal characteristics of hemodynamic and metabolic response

The temporal characteristics of the measured hemodynamic responses are consistent with previous measurements during both forepaw and whisker stimulation in rats. For example, the time to peak amplitude of the measured response of each parameter in Fig. 6 is consistent with the measurements of Jones et al. (2001), who used concurrent slit spectroscopy to determine the temporal response of HbO, HbR, and HbT, and point measurements of CBF using laser Doppler flowmetry. The timecourses of the CBF changes are also consistent with those of Ances et al. (2001) for forepaw stimulation, where an initial peak in CBF was observed, followed by a prolonged secondary plateau of lower amplitude.

The CMRO₂ timecourse shows a similar trend with an initial peak and a secondary plateau, although the amplitude of the secondary plateau relative to the peak response is smaller than that of CBF. For forepaw stimulation, for example, the secondary plateau of CBF is approximately 0.5 times the peak CBF response while the secondary plateau in CMRO₂ is only 0.2 times its peak value. The relative amplitudes of the secondary plateaus of the CBF and CMRO₂ changes are very similar to those reported by Ances et al. (2001), who calculated CMRO₂ changes from measurements of CBF using laser Doppler flowmetry and oxygen tension measurements. These results indicate that CBF and CMRO₂ changes are closely related during the early stages of the stimulus but have a different relationship during the latter part of a prolonged stimulus, suggesting that a strict coupling relationship between flow and oxygen consumption may not exist at all times.

The existence of an early increase in oxygen consumption, or the ‘initial dip’, has been controversial. While some studies have reported an initial rise in HbR concentrations, others have reported no such early changes in either HbR or CMRO₂ (Kohl et al., 2000; Sheth et al., 2004a). We found no observable early changes in either HbR or CMRO₂ that preceded a flow change for either forepaw or whisker stimulation in an average of 40 individual trials. However, since the amplitude of the initial dip may be very small, a very high contrast to noise ratio may be required to detect the early changes. Indeed, we observed an initial dip in our previous studies that utilized an event-related presentation of brief stimuli, and a large number of stimulus presentation trials (Devor et al., 2003, 2005).

Another parameter commonly used to assess the coupling between CBF and CMRO₂ is the ratio of the changes of each parameter, i.e., the flow consumption ratio $\Delta\text{CBF}/\Delta\text{CMRO}_2$.

Various studies have determined this ratio to be in the range of 2–5 (Ances et al., 2001; Davis et al., 1998; Fox et al., 1988). We have found this ratio to be 1.5 and 2.0 for the peak response to forepaw and whisker stimulation, respectively, and these values are close to those reported in studies involving rodents (Ances et al., 2001; Davis et al., 1998; Fox et al., 1988). Importantly, we note that the flow consumption ratio can vary in time as the ratio increases to 4.5 and 2.5, respectively, during the plateau phase. These values are consistent with those reported by Ances et al., who found values of 1.0 and 2.93 for the peak and plateau phases of forepaw stimulation (Ances et al., 2001).

Flow/volume relationship

The relationship between the changes in CBF and CBV is often assumed to follow the Grubb relation (Buxton and Frank, 1997; Grubb et al., 1974), $\text{CBV} = \text{CBF}^\phi$, where the coefficient ϕ has been found to be in the range of 0.18–0.38 (Jones et al., 2001, 2002; Mandeville et al., 1999; Sheth et al., 2004b). We determined ϕ to be 0.25 ± 0.03 for forepaw stimulation and 0.20 ± 0.03 for whisker stimulation, when averaged over the time $4 < t < 8$ s within a 2-mm region of interest centered on the response. These values are somewhat lower than those found by Grubb et al. (1974) in monkeys, although they are consistent with previous measurements of stimulation-induced changes in rodents (Jones et al., 2001, 2002; Mandeville et al., 1999; Sheth et al., 2004a).

To examine whether a spatial dependence exists on the relationship between CBF and CBV, ϕ was calculated within a series of concentric rings centered on the activation and averaged over the same time interval (4–8 s). Fig. 11 illustrates that a slight spatial dependence exists, and ϕ is greatest near the center of activation, and decreases at distances further away from the center. Beyond approximately 1 mm from the center of activation, ϕ begins to increase perhaps due to noise as the amplitudes of the changes in both HbT and CBF are significantly smaller. This initial decrease in ϕ with increasing distance from the center of activation may indicate that arterial dilation occurs primarily in the center of the activation such that the amplitude of the HbT changes relative to the CBF changes is greater near the center of activation, although the spatial extents of both HbT and CBF likely exceed the spatial extent of the neuronal activity. These results illustrate one of the advantages of obtaining the full spatiotemporal dynamics of both blood flow and blood oxygenation.

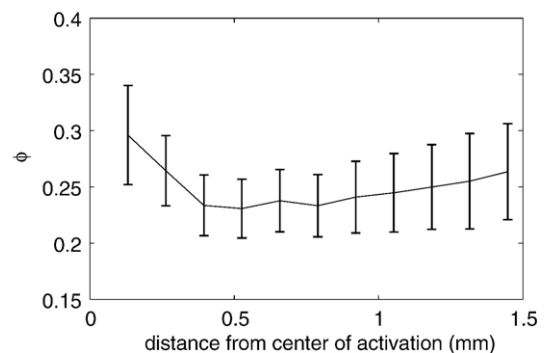


Fig. 11. Spatial variation in ϕ ($\text{CBV} = \text{CBF}^\phi$) during forepaw stimulation. ϕ was calculated in a series of concentric rings centered on the activation, and the average value of ϕ is plotted vs. distance from the center of activation.

Conclusions

Developing a better understanding of the spatiotemporal characteristics of the hemodynamic and CMRO₂ response to functional activation is important for furthering our understanding of the complex neurovascular coupling relationships. In this study, laser speckle contrast imaging of CBF was combined with multi-wavelength optical reflectance imaging to compare the spatial extents of the hemodynamic and oxygen metabolism changes due to forepaw and whisker stimulation in rats. The spatial extents of the responses of each hemodynamic parameter and CMRO₂ at the time of peak response were found to be comparable. This result suggests that although the CMRO₂ response is a metabolic measure, it does not necessarily have a smaller spatial extent than the purely hemodynamic measures of HbO, Hb, HbT, and CBF. However, since the CMRO₂ response has different temporal dynamics than the purely hemodynamic measures, it reveals unique information about the response to functional activation and full field imaging of HbO, HbR, HbT, CBF, and CMRO₂ changes provides a more complete picture of the hemodynamic response.

Acknowledgments

The authors acknowledge support from the National Institutes of Health (NS41291, NS050150, and EB000790) and the Whitaker Foundation.

References

- Ances, B.M., Greenberg, J.H., et al., 1999. Laser doppler imaging of activation–flow coupling in the rat somatosensory cortex. *Neuroimage* 10 (6), 716–723.
- Ances, B.M., Wilson, D.F., et al., 2001. Dynamic changes in cerebral blood flow, O₂ tension, and calculated cerebral metabolic rate of O₂ during functional activation using oxygen phosphorescence quenching. *J. Cereb. Blood Flow Metab.* 21 (5), 511–516.
- Ayata, C., Dunn, A.K., et al., 2004. Laser speckle flowmetry for the study of cerebrovascular physiology in normal and ischemic mouse cortex. *J. Cereb. Blood Flow Metab.* 24 (7), 744–755.
- Ba, A.M., Guiou, M., et al., 2002. Multiwavelength optical intrinsic signal imaging of cortical spreading depression. *J. Neurophysiol.* 88 (5), 2726–2735.
- Bevilacqua, F., Pigué, D., et al., 1999. In vivo local determination of tissue optical properties: applications to human brain. *Appl. Opt.* 38 (22), 4939–4950.
- Bolay, H., Reuter, U., et al., 2002. Intrinsic brain activity triggers trigeminal meningeal afferents in a migraine model. *Nat. Med.* 8 (2), 136–142.
- Bonner, R., Nossal, R., 1981. Model for laser Doppler measurements of blood flow in tissue. *Appl. Opt.* 20, 2097–2107.
- Brett-Green, B.A., Chen-Bee, C.H., et al., 2001. Comparing the functional representations of central and border whiskers in rat primary somatosensory cortex. *J. Neurosci.* 21 (24), 9944–9954.
- Briers, J.D., 2001. Laser Doppler, speckle and related techniques for blood perfusion mapping and imaging. *Physiol. Meas.* 22 (4), R35–R66.
- Briers, J.D., Richards, G., et al., 1999. Capillary blood flow monitoring using laser speckle contrast analysis. *J. Biomed. Opt.* 4, 164–175.
- Buxton, R.B., Frank, L.R., 1997. A model for the coupling between cerebral blood flow and oxygen metabolism during neural stimulation. *J. Cereb. Blood Flow Metab.* 17 (1), 64–72.
- Buxton, R.B., Wong, E.C., et al., 1998. Dynamics of blood flow and oxygenation changes during brain activation: the balloon model. *Magn. Reson. Med.* 39 (6), 855–864.
- Culver, J.P., Durduran, T., et al., 2003. Diffuse optical tomography of cerebral blood flow, oxygenation, and metabolism in rat during focal ischemia. *J. Cereb. Blood Flow Metab.* 23 (8), 911–924.
- Davis, T.L., Kwong, K.K., et al., 1998. Calibrated functional MRI: mapping the dynamics of oxidative metabolism. *Proc. Natl. Acad. Sci. U. S. A.* 95, 1834–1839.
- Devor, A., Dunn, A.K., et al., 2003. Coupling of total hemoglobin concentration, oxygenation, and neural activity in rat somatosensory cortex. *Neuron* 39 (2), 353–359.
- Devor, A., Ulbert, I., et al., 2005. Coupling of the cortical hemodynamic response to cortical and thalamic neuronal activity. *Proc. Natl. Acad. Sci. U.S.A.* 102 (10), 3822–3827.
- Dunn, A.K., Bolay, H., et al., 2001. Dynamic imaging of cerebral blood flow using laser speckle. *J. Cereb. Blood Flow Metab.* 21 (3), 195–201.
- Dunn, A.K., Devor, A., et al., 2003. Simultaneous imaging of total cerebral hemoglobin concentration, oxygenation, and blood flow during functional activation. *Opt. Lett.* 28, 28–30.
- Durduran, T., Burnett, M.G., et al., 2004a. Spatiotemporal quantification of cerebral blood flow during functional activation in rat somatosensory cortex using laser-speckle flowmetry. *J. Cereb. Blood Flow Metab.* 24 (5), 518–525.
- Durduran, T., Yu, G., et al., 2004b. Diffuse optical measurement of blood flow, blood oxygenation, and metabolism in a human brain during sensorimotor cortex activation. *Opt. Lett.* 29 (15), 1766–1768.
- Durham, D., Woolsey, T.A., 1985. Functional organization in cortical barrels of normal and vibrissae-damaged mice: a (3H) 2-deoxyglucose study. *J. Comp. Neurol.* 235 (1), 97–110.
- Erinjeri, J.P., Woolsey, T.A., 2002. Spatial integration of vascular changes with neural activity in mouse cortex. *J. Cereb. Blood Flow Metab.* 22 (3), 353–360.
- Fabricius, M., Akgoren, N., et al., 1997. Laminar analysis of cerebral blood flow in cortex of rats by laser-Doppler flowmetry: a pilot study. *J. Cereb. Blood Flow Metab.* 17 (12), 1326–1336.
- Fox, P.T., Raichle, M.E., 1986. Focal physiological uncoupling of cerebral blood flow and oxidative metabolism during somatosensory stimulation in human subjects. *Proc. Natl. Acad. Sci. U. S. A.* 83 (4), 1140–1144.
- Fox, P.T., Raichle, M.E., et al., 1988. Nonoxidative glucose consumption during focal physiologic neural activity. *Science* 241 (4864), 462–464.
- Gerrits, R.J., Raczynski, C., et al., 2000. Regional cerebral blood flow responses to variable frequency whisker stimulation: an autoradiographic analysis. *Brain Res.* 864 (2), 205–212.
- Graaff, R., Aarnoose, J.G., et al., 1992. Reduced light-scattering properties for mixtures of spherical particles: a simple approximation derived from Mie calculations. *Appl. Opt.* 31, 1370–1376.
- Grinvald, A., Lieke, E., et al., 1986. Functional architecture of cortex revealed by optical imaging of intrinsic signals. *Nature* 324, 361–364.
- Grinvald, A., Lieke, E.E., et al., 1994. Cortical point-spread function and long-range lateral interactions revealed by real-time optical imaging of macaque monkey primary visual cortex. *J. Neurosci.* 14 (5 Pt. 1), 2545–2568.
- Grubb, R.L. Jr., Raichle, M.E., et al., 1974. The effects of changes in PaCO₂ on cerebral blood volume, blood flow, and vascular mean transit time. *Stroke* 5 (5), 630–639.
- Hoge, R.D., Atkinson, J., et al., 1999. Linear coupling between cerebral blood flow and oxygen consumption in activated human cortex. *Proc. Natl. Acad. Sci. U. S. A.* 96 (16), 9403–9408.
- Hoge, R.D., Franceschini, M.A., et al., 2005. Simultaneous recording of task-induced changes in blood oxygenation, volume, and flow using diffuse optical imaging and arterial spin-labeling MRI. *NeuroImage* 25 (3), 701–707.
- Hyder, F., 2004. Neuroimaging with calibrated FMRI. *Stroke* 35 (11 Suppl. 1), 2635–2641.
- Hyder, F., Shulman, R.G., et al., 1998. A model for the regulation of cerebral oxygen delivery. *J. Appl. Physiol.* 85 (2), 554–564.
- Jones, M., Berwick, J., et al., 2001. Concurrent optical imaging spectroscopy and laser-Doppler flowmetry: the relationship between blood

- flow, oxygenation, and volume in rodent barrel cortex. *Neuroimage* 13 (6 Pt. 1), 1002–1015.
- Jones, M., Berwick, J., et al., 2002. Changes in blood flow, oxygenation, and volume following extended stimulation of rodent barrel cortex. *Neuroimage* 15 (3), 474–487.
- Kharlamov, A., Brown, B.R., et al., 2004. Heterogeneous response of cerebral blood flow to hypotension demonstrated by laser speckle imaging flowmetry in rats. *Neurosci. Lett.* 368 (2), 151–156.
- Kida, I., Kennan, R.P., et al., 2000. High-resolution CMR(O₂) mapping in rat cortex: a multiparametric approach to calibration of BOLD image contrast at 7 Tesla. *J. Cereb. Blood Flow Metab.* 20 (5), 847–860.
- Kleinfeld, D., Delaney, K.R., 1996. Distributed representation of vibrissa movement in the upper layers of somatosensory cortex revealed with voltage-sensitive dyes. *J. Comp. Neurol.* 375 (1), 89–108.
- Kohl, M., Lindauer, U., et al., 2000. Physical model for the spectroscopic analysis of cortical intrinsic optical signals. *Phys. Med. Biol.* 45 (12), 3749–3764.
- Kossut, M., Hand, P.J., et al., 1988. Single vibrissal cortical column in SI cortex of rat and its alterations in neonatal and adult vibrissa-deafferented animals: a quantitative 2DG study. *J. Neurophysiol.* 60 (2), 829–852.
- Lu, H., Golay, X., et al., 2003. Functional magnetic resonance imaging based on changes in vascular space occupancy. *Magn. Reson. Med.* 50 (2), 263–274.
- Malonek, D., Grinvald, A., 1996. Interactions between electrical activity and cortical microcirculation revealed by imaging spectroscopy: implications for functional brain mapping. *Science* 272 (5261), 551–554.
- Mandeville, J.B., Marota, J.J., et al., 1999. Evidence of a cerebrovascular postarteriole windkessel with delayed compliance. *J. Cereb. Blood Flow Metab.* 19 (6), 679–689.
- Masino, S., Frostig, R., 1996. Quantitative long-term imaging of the functional representation of a whisker in rat barrel cortex. *Proc. Natl. Acad. Sci. U. S. A.* 93, 4942–4947.
- Masino, S., Kwon, M., et al., 1993. Characterization of functional organization within rat barrel cortex using intrinsic signal optical imaging through a thinned skull. *Proc. Natl. Acad. Sci. U. S. A.* 90, 9998–10002.
- Matcher, S.J., Cope, M., et al., 1997. In vivo measurements of the wavelength dependence of tissue-scattering coefficients between 760 and 900 nm measured with time-resolved spectroscopy. *Appl. Opt.* 36 (1), 386–396.
- Mayhew, J., Johnston, D., et al., 2000. Spectroscopic analysis of neural activity in brain: increased oxygen consumption following activation of barrel cortex. *Neuroimage* 12 (6), 664–675.
- Mayhew, J., Johnston, D., et al., 2001. Increased oxygen consumption following activation of brain: theoretical footnotes using spectroscopic data from barrel cortex. *Neuroimage* 13 (6 Pt. 1), 975–987.
- McCasland, J.S., Woolsey, T.A., 1988. High-resolution 2-deoxyglucose mapping of functional cortical columns in mouse barrel cortex. *J. Comp. Neurol.* 278 (4), 555–569.
- Saad, Z.S., Ropella, K.M., et al., 2003. The spatial extent of the BOLD response. *Neuroimage* 19 (1), 132–144.
- Sheth, S., Nemoto, M., et al., 2003. Evaluation of coupling between optical intrinsic signals and neuronal activity in rat somatosensory cortex. *Neuroimage* 19 (3), 884–894.
- Sheth, S.A., Nemoto, M., et al., 2004a. Columnar specificity of microvascular oxygenation and volume responses: implications for functional brain mapping. *J. Neurosci.* 24 (3), 634–641.
- Sheth, S.A., Nemoto, M., et al., 2004b. Linear and nonlinear relationships between neuronal activity, oxygen metabolism, and hemodynamic responses. *Neuron* 42 (2), 347–355.
- Slovin, H., Arieli, A., et al., 2002. Long-term voltage-sensitive dye imaging reveals cortical dynamics in behaving monkeys. *J. Neurophysiol.* 88 (6), 3421–3438.
- Strangman, G., Franceschini, M.A., et al., 2003. Factors affecting the accuracy of near-infrared spectroscopy concentration calculations for focal changes in oxygenation parameters. *Neuroimage* 18 (4), 865–879.
- Tootell, R.B., Switkes, E., et al., 1988. Functional anatomy of macaque striate cortex: II. Retinotopic organization. *J. Neurosci.* 8 (5), 1531–1568.
- Tootell, R.B., Mendola, J.D., et al., 1997. Functional analysis of V3A and related areas in human visual cortex. *J. Neurosci.* 17 (18), 7060–7078.
- Ts'o, D.Y., Frostig, R.D., et al., 1990. Functional organization of primate visual cortex revealed by high resolution optical imaging. *Science* 249 (4967), 417–420.